Project No. 12-4026

Electrochemical Corrosion Studies for Modeling Metallic Waste Form Release Rates

Fuel Cycle Research and Development

Frederic Poineau
University of Nevada, Las Vegas

In collaboration with:
Florida Memorial University

Kimberly Gray, Federal POC
William Ebert, Technical POC

NEUP Nuclear Energy University Programs
U.S. Department of Energy

Final report

Electrochemical Corrosion Studies for Modeling Metallic Waste Form Release Rates

Technical work scope Identifier No: Separations and Waste Forms (FC-1) and Used Nuclear Fuel Disposition (FC-4)

Frederic Poineau, Romina Farmand, Erik Johnstone, Eunja Kim, Ken Czerwinski (University of Nevada, Las Vegas)
Dr. Gordon Jarvinen, Dr. Dave Kolman (Los Alamos National Laboratory)
Prof. Dimitri Tamalis (Florida Memorial University)

1. Background and objectives

The isotope ^{99}Tc is an important fission product generated from nuclear power production. Because of its long half-life ($t_{1/2} = 2.13.10^5$ years) and beta-radiotoxicity (β^-= 292 keV), it is a major concern in the long-term management of spent nuclear fuel.[1] In the spent nuclear fuel, Tc is present as an alloy with Mo, Ru, Rh, and Pd called the epsilon-phase, the relative amount of which increases with fuel burn-up.[2] In some separation schemes for spent nuclear fuel, Tc would be separated from the spent fuel and disposed of in a durable waste form.[3] Technetium waste forms under consideration include metallic alloys, oxide ceramics and borosilicate glass.[4, 5] In the development of a metallic waste form, after separation from the spent fuel, Tc would be converted to the metal, incorporated into an alloy and the resulting waste form stored in a repository.[6] Metallic alloys under consideration include Tc-Zr alloys, Tc-stainless-steel alloys and Tc-Inconel alloys (Inconel is an alloy of Ni, Cr and iron which is resistant to corrosion).

To predict the long term behavior of the metallic Tc waste form, understanding the corrosion properties of Tc metal and Tc alloys in various chemical environments is needed but efforts to model the behavior of Tc metallic alloys are limited. [7]

One parameter that should also be considered in predicting the long-term behavior of the Tc waste form, is the ingrowth of stable Ru that occurs from the radioactive decay of ^{99}Tc ($^{99}Tc \rightarrow {}^{99}Ru + \beta^-$). After a geological period of time, significant amount of Ru will be present in the Tc and may affect its corrosion properties. Studying the effect of Ru on the corrosion behavior of Tc is also of importance.

In this context, we studied the electrochemical behavior of Tc metal, Tc-Ni alloys (to model Tc-Inconel alloy) and Tc-Ru alloys in acidic media. The study of Tc-U alloys has also been performed in order to better understand the nature of Tc in metallic spent fuel. Computational modeling and simulations were performed to shed light on experimental results and explain structural and kinetics trends. The project consisted of three tasks:

Task 1: Preparation and characterization of Tc containing alloys

Technetium metal, Tc-Ni, Tc-Ru and Tc-U alloys were prepared and characterized by scanning electron microscopy (SEM), electron dispersive X-ray spectroscopy (EDX) and electron probe micro analysis (EPMA). Following their preparation, the alloys were mounted into electrodes.

Task 2: Corrosion studies

The electrochemical behavior of the alloys (exception of Tc-U alloys) prepared in Task 1 was studied in acidic media (HNO_3 or H_2SO_4) at room temperature. The electrochemical methods include linear voltammetry, open circuit potential and polarization resistance measurements. The speciation of Tc in solution after electrochemical corrosion of Tc-Ru alloys was performed by UV-Visible spectroscopy and electrospray induction-mass spectroscopy.

Task 3: Computational studies

Computational studies (DFT) were carried out to investigate structural and mechanical and surface properties of Tc metal, Tc-Ru alloys and Tc-Fe-oxides; the theoretical results were compared to the experimental one. The surface chemistry of Tc

metal relative to hydrogen, oxygen and water molecule adsorption was studied; those studies allowed a better understanding of the corrosion of Tc metal.

2. Results of Task 1

2.1. Preparation and characterization of Tc-Ru alloys and electrodes.

Technetium metal was prepared from the reduction NH_4TcO_4 under H5 (5 % hydrogen/ 95 % argon) atmosphere at 750 ^oC for 2 hours. Ruthenium metal (99.99 %) powder was purchased from Alfa-Aesar.

Technetium and Ru metal powders were weighted and grounded in a mortar. The compositions were chosen in order to simulate Tc-Ru alloys obtained from the decay of Tc at various periods of time (Table 1). Because Tc and Ru have hexagonal close-packed (hcp) structures and similar size, they are fully miscible and form complete hcp solid solutions. After grinding, Tc-Ru powder mixtures were placed in a 6 mm die and pressed for 10 minutes at 4 tons. The cylindrical pellets were arc melted under an argon atmosphere and the resulting metallic beads were annealed at 1700 °C under H5 atmosphere for 12 hours.

The resulting beads were imbedded in a conductive epoxy and polished with silicon carbide disk papers (220 grit and 1200 grit) and with diamond abrasives (9 µm, 3 µm and 1 µm). The alloys were characterized by SEM, EDX mapping and EPMA analysis were performed; all the alloys exhibit a single phase. EDX mapping on indicates the alloys to be homogenous solid solutions; the compositions of the alloys determined by EPMA are presented in Table 1. The SEM images of the samples are presented in Fig. 1 to 3.

After EPMA, the metallic beads were removed from the conductive epoxy and washed with acetone and water. The beads were connected to a copper rod (1 mm diameter, 8 cm length) with silver epoxy and then dried for 24 hours (Fig. 4). The resulting metallic beads attached to a copper rod with silver epoxy were inserted in a plastic tube (6.5 mm diameter, 8 cm length) and sealed with a temperature/acid/base epoxy resin. After 24 hours, each electrode was removed from the tubing and their surface determined by SEM (Table 1).

Table 1. Experimental compositions of Tc-Ru alloys and the time required to produce the amount of Ru from the decay of ^{99}Tc. The surface of the electrode is also presented.

Samples	Experimental compositions Tc: Ru (at. %)	Electrode surface (mm^2)	Decay time (years)
a	96.8: 3.2	2.47	9 995
b	94.8: 5.2	2.62	16 410
c	79.9: 20.1	2.61	68 960
d	75.3: 24.7	2.90	87 180

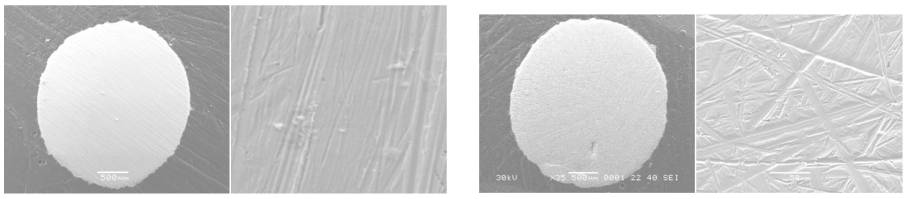

Fig. 1. SEM image of samples a (left) and b (right). Magnification of x35 and x500

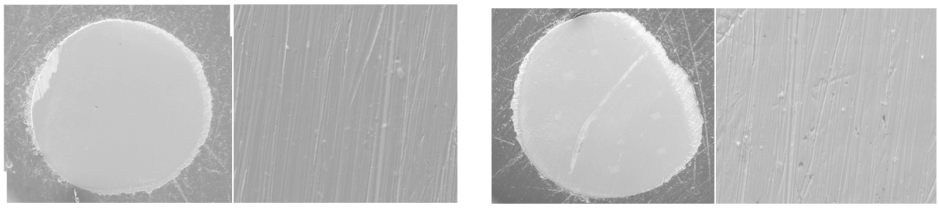

Fig. 2. SEM image of samples c (left) and d (right). Magnification of x35 and x500

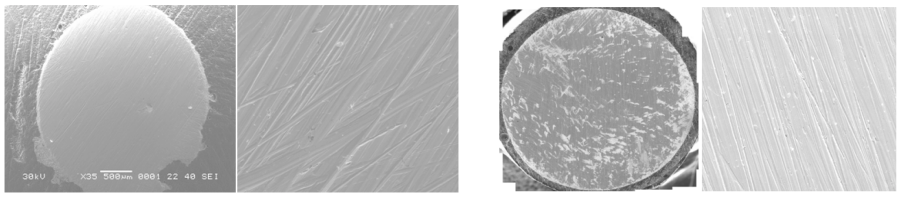

Fig. 3. SEM image of metallic Tc (left) and Ru (right). Magnification of x35 and x500

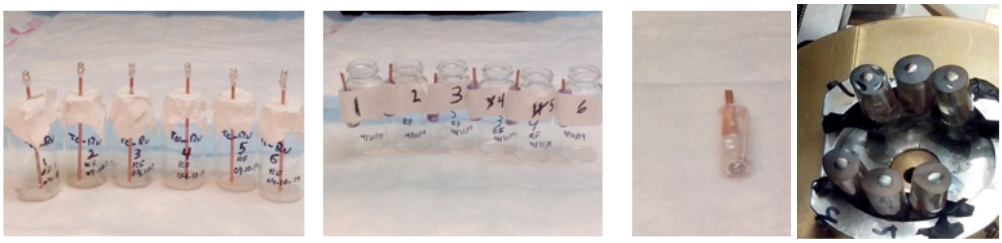

Fig. 4. Preparation of Tc-Ru electrodes. Tc-Ru electrodes on SEM samples holder (right)

2.2. Technetium-Ni alloys preparation.

Three different Tc-Ni alloys were made. Mixtures of Tc and pure Ni powders were weighed out containing 1 and 10 wt% Tc.

The mixed solids were ground manually for 3-5 minutes, transferred to a 6 mm diameter stainless steel die and pressed at 4 tons for 10 minutes at room temperature. The resulting alloys were treated at 1050 °C and 1550 °C. Specimens were mounted in epoxy and polished to a 600-grit finish and ultrasonically cleaned in ethanol for five minutes. SEM analysis suggests that the 1550 ^{o}C heat treatment was sufficient to alloy the materials. Cold pressed ("As-pressed") and 1050 ^{o}C samples retained distinct islands of Tc metal within the Ni matrix.

Sintering powder might simplify the development of waste form by lowering the temperature of preparation. For this, the sintering temperature needs to be above the melting point of the main component. In our case, one sintering temperature (1550 °C)

was above the meting point of Ni (1455 °C); as expected, the resulting material was in the form of Tc metal embedded within a Ni matrix.

2.3 Technetium-U alloys

Currently, only two Tc-U alloys have been reported in the literature, i.e., U_2Tc and UTc_2,.[8] Because Tc is a major fission product (~6% fission yield) and this system is much less understood than the ones of Re and Ru, it was an area of combined actinide and transition metal chemistry to be further explored. U-Tc alloys with varying stoichiometries (Table 2) were synthesized. The theoretical compositions were based of the U-M (M = Ru, Re) systems.

The "U_2Tc" sample was analyzed by PXRD and SEM/EDX spectroscopy. The XRD powder pattern shows the sample to be semi-crystalline and no crystallographic information could be extracted. The SEM analysis shows the sample to contain a single phase (Fig.5). The EDX data analysis (Fig. 6. and Table 3) shows the sample to have the experimental composition $U_{64.77}Tc_{35.23}$ which is consistent with the U_2Tc stoichiometry.

Table 2. Stoichiometries, atomic percentages, and masses of U and Tc used in the preparation of U-Tc alloys.

Theoretical Compositions	U at.%	Tc at.%	U (mg)	Tc (mg)
U_2Tc	67	33	207.5	42.5
UTc	50	50	176.6	73.4
UTc_2	33	67	135.6	114.4
UTc_3	25	75	111.4	138.6

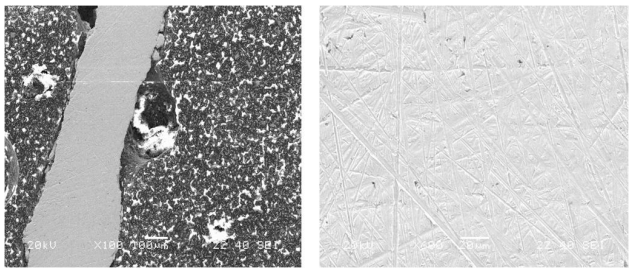

Fig. 5. SEM image of U_2Tc alloys. Magnifications x100 (left) and x600 (right)

Table 3. Stoichiometry of the "U_2Tc" sample determined by EDX

Element	Weight%	Atomic%
Tc	18.64	35.52

U	81.36	64.48

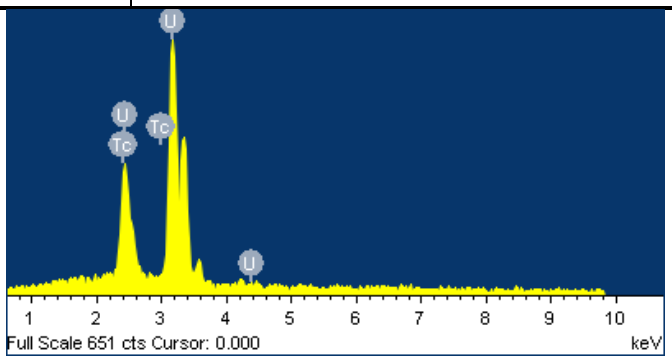

Fig. 6. EDX spectra of the U_2Tc sample after treatment at 900 °C for 2 weeks.

3. Results of Task 2

3.1. Corrosion studies of Tc metal

Electrochemical studies of Tc metal were performed in H_2SO_4 (pH = 3.2) at room temperature. The experimental set-up consisted of an electrochemical cell (100 mL) incorporating an Ag/AgCl reference electrode and a platinized-niobium mesh counter electrode. In this study, the potentials are referenced *vs* NHE. The Tc electrode was connected to a Bio-Logic potentiostat (Model SP-200). Prior to polarization, working electrodes were immersed in solution for four hours and the open circuit potential monitored. Potentiodynamic polarization tests were performed using a scan rate of 0.1 mV/s.

Open circuit potential measurements for Tc metal are presented in Fig. 7. Data are superimposed on the potential – pH diagram for Tc. The red and black lines represent two different published values for the TcO_2 / TcO_4^- transition. The open circuit potential (0.4-0.55 V) appears to fall near or above the transition. The TcO_4^- region is a region of corrosion (as opposed to passivity), therefore pure Tc metal would not be predicted to spontaneously passivate upon exposure to H_2SO_4 pH = 3.2 Anodic polarization measurements (Fig.8) were performed in the range OCP_{4h} to 0.78 V; results confirm that Tc does not passivate in H_2SO_4 at pH = 3.2

Although not observed on the forward scan, the reverse scan indicates a transition that may be the TcO_2 / TcO_4^- transition. This transition appears at a potential more noble than that reported in the literature. The discrepancy may be attributable to the reported sluggishness of the TcO_2 / TcO_4^- reaction.

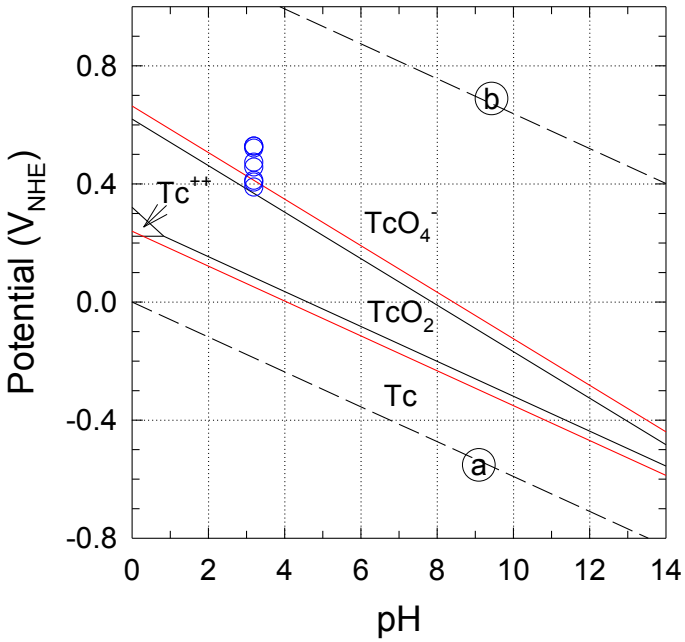

Fig. 7. Open circuit potential data of Tc metal following 4 hours exposure in H_2SO_4 at pH = 3.2.

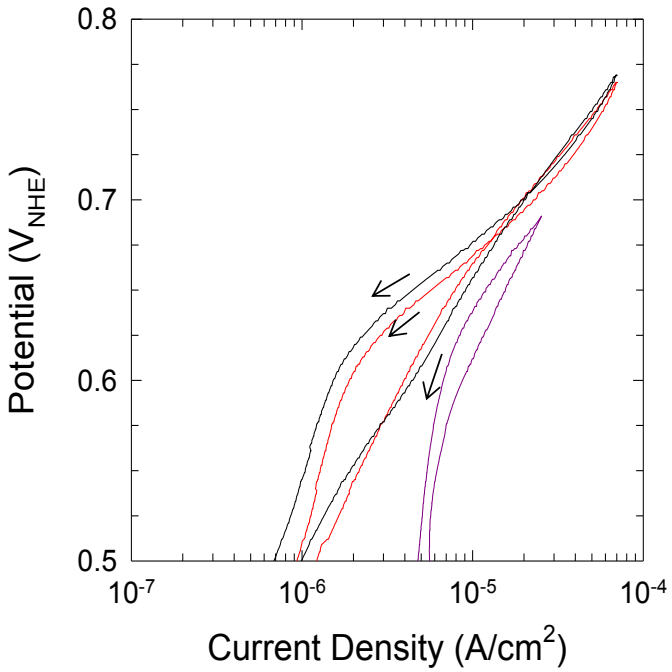

Fig. 8. Anodic polarization curves for Tc metal exposed to H_2SO_4 at pH = 3.2.

3.2. Technetium-Ru alloys corrosion studies

Those electrochemical studies were performed in a three-electrode electrochemical cell. The volume of the solution used in those studies was 9 mL. The three-electrode

configuration consisted of a reference electrode (Ag/AgCl), a working electrode (Tc-Ru alloys) and an auxiliary electrode (Pt wire, 0.5 mm diameter). The electrodes were connected to a CH Instruments, Inc., potentiostat CHI660b controlled by a computer. Prior to electrochemical measurements, the electrodes were polished with 220 grit silicon carbide paper and rinsed with methanol and DI H_2O. In this study, the potentials are referenced *vs* Ag/AgCl and the measurements were performed at 22 °C. The electrochemical behavior of Tc, Ru metals and Tc-Ru alloys (Table 1) in nitric acid solutions were studied by linear voltammnetry.

UV-Visible measurements were performed on a Cary 6000i UV-Vis-NIR spectrophotometer between 800 and 300 nm in a 1 cm pathlength quartz cuvette, 1 M HNO_3 was used as the baseline solvent. Electrospray ionization-mass spectrometry measurements were performed on Dionex MSQ plus Electrospray ionization with a quadrupole mass filter detector. The solution samples were introduced in a capillary and then diluted in a carrier solvent (DI H_2O).

Study of Tc-Ru alloys. The Tc-Ru electrodes were immersed in 1 M HNO_3 and the potentials were scanned (10 $mV.s^{-1}$) from 0.2 to 1.2 V (Fig. 9). During the experiment, no gas evolution was observed for all the samples. On the voltammogramms, only anodic currents were observed. The absence of cathodic currents indicate that the reduction of $NO_3^-$to HNO_2 is not a significant process and that HNO_2 should not play a role on the speciation of Tc and Ru in the domain of potential studied.

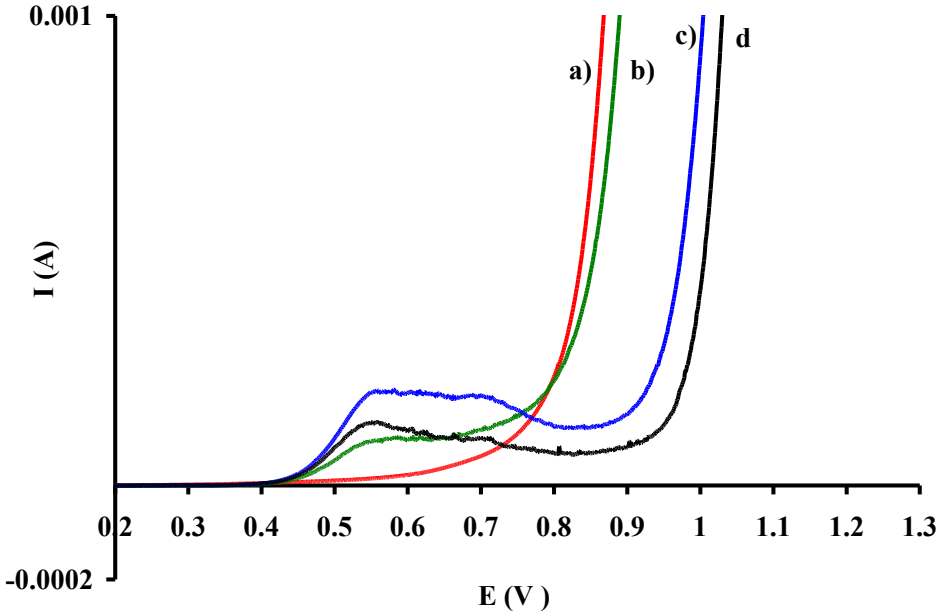

Fig. 9. Linear voltammograms (10 $mV.s^{-1}$) of Tc-Ru alloys electrodes in 1 M HNO_3. a) sample a in red; b) sample b in green; c) sample c in black and d) sample d in blue.

The transpassivation potentials of the alloys were determined by extrapolation of the linear part of the voltammogram. A representation of the extrapolation for Tc metal is presented in Fig 10. Results (Table 4) show that the E_{TP} increase with the Ru content which indicates better corrosion resistance. A similar phenomenon has been previously

observed for Tc-Ru alloys (Ru = 19, 45, 70 at. %) in 1 M HNO_3 where the dissolution potentials were respectively 0.93, 1.08 and 1.13 V.[9] The representation of the E_{TP} as the function of the Ru content is presented in Fig. 11 and in Fig. 12 for Ru content below 6 at. %.

Analysis of Fig. 12 shows that a linear relationship (Equation 1) between the value of E_{TP} and the Ru content is observed. Equation 1 indicates that for Ru < 6 at. %, the E_{TP} increases by ~16 mV for every atomic % of Ru.

$E_{TP} = 0.0165.\ Ru + 0.665$ Equation 1

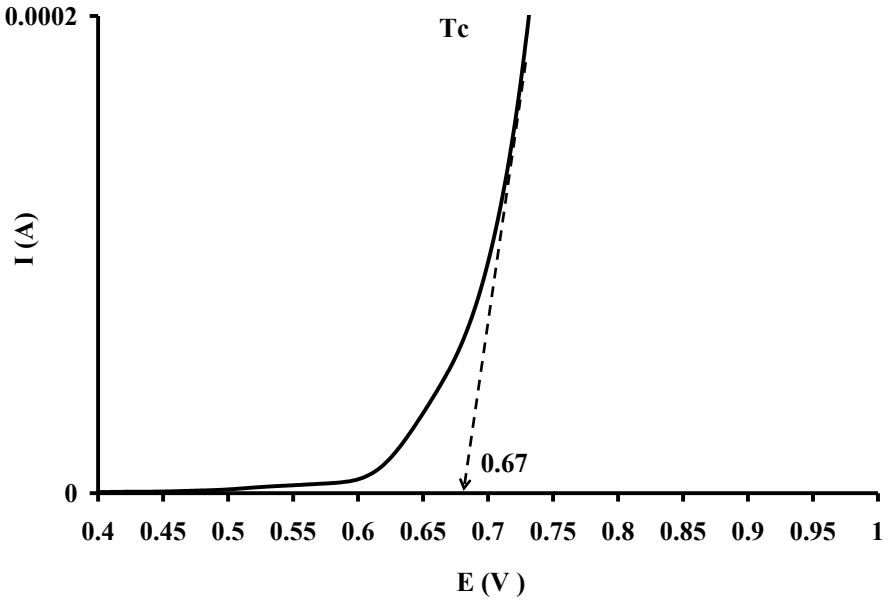

Fig. 10. Linear voltammogram of Tc metal in 1 M HNO_3 (scan rate = 10 $mV.s^{-1}$). The dashed line represent the extrapolation to i = 0 of the linear part.

Table 4. Values of E_{TP} (V) for Tc, Ru and samples (a-d) in 1 M HNO_3. Uncertainty on E_{TP} is ± 10 mV.

Sample	**E_{TP} (V)**	**Sample**	**E_{TP} (V)**
Tc	0.67	c	0.92
a	0.72	d	0.96
b	0.75	Ru	1.14

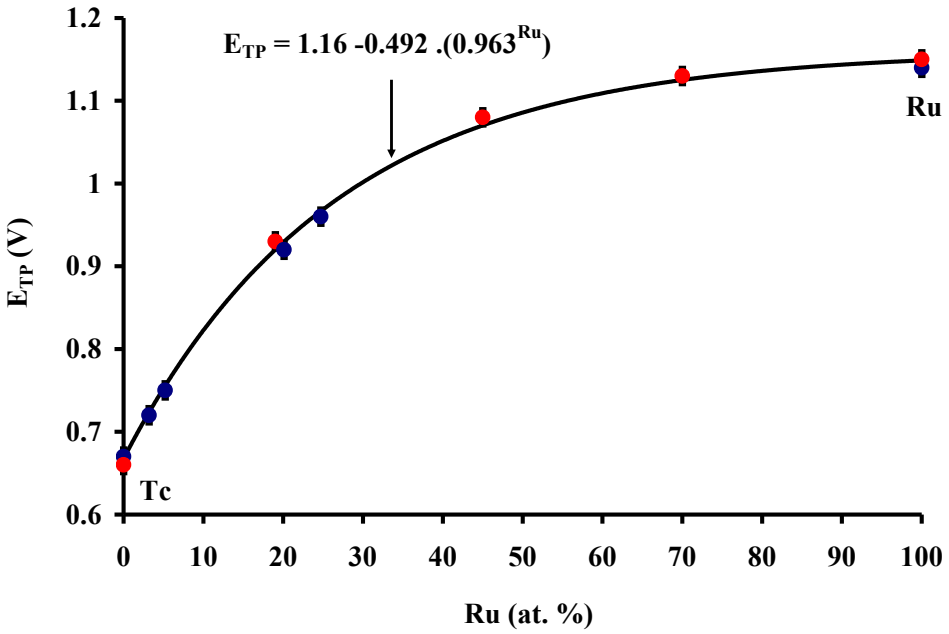

Fig. 11. Representation of the E_{TP} in 1 M HNO_3 as a function of Ru content (at. %) in Tc-Ru alloys. In blue, values determined in this work. In red, values determined in [9]. The solid curve represent the best fit of the function E_{TP} = f (Ru); the equation of the curve is also displayed.

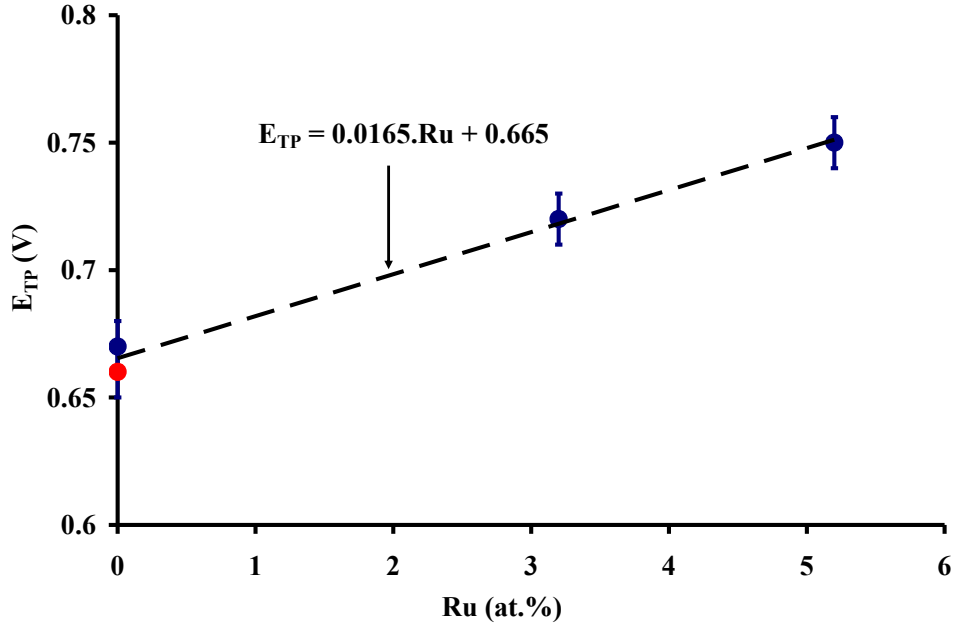

Fig. 12. Representation of the E_{TP} in 1 M HNO_3 for Ru below 6 at. %. In blue, values determined in this work. In, red values determined in [9]. The dashed line represent the best linear fit of the function E_{TP} = f (Ru); the equation of the line is also displayed.

For nuclear applications, it is of interest to predict the value of E_{TP} as a function of the decay time. In order to performed those predictions, the transpassivation potentials of the Tc-Ru alloys (E_{TP}) as a function of the Ru content in the alloys (Ru%) was fitted with a mathematical function. The best fit (Fig.11, solid curve) was obtained using an exponential function (Equation 2).

Because the amount of ^{99}Ru produce by decay of ^{99}Tc is a function of the time, a relation (Equation 4) between E_{TP} and the decay time can be derived by taking the logarithm of the Equation 2 (Equation 3) and replacing Ru(t) by $100(1-e^{-\lambda.t})$ in Equation 3. In those equations, t is the decay time and λ =Ln(2)/213 000.

$$E_{TP}= 1.16 -0.492.(0.963^{Ru}) \quad \text{Equation 2}$$

$$Ln[1.16-E_{TP}] =Ln(0.492) + Ru(t).\ Ln(0.963) \quad \text{Equation 3}$$

$$Ln[1.16-E_{TP}] = -4.479 + 3.770e^{(-\lambda.t)} \quad \text{Equation 4}$$

Using Equation 4, the value of E_{TP} of Tc in 1 M HNO_3 after 1 000, 10 000, 100 000 years and one half-life of Tc can be estimated (Table 5). For decay time of 1 000 and 10 000 years, the E_{TP} values are comparable to the one of Tc while after one Tc half-life, the values are comparable to the one of Ru.

Table 5. Estimated value of E_{TP} (V) as a function of the decay time (years)

Decay time	E_{TP}	Decay time	E_{TP}
1 000	0.67	100 000	0.99
10 000	0.72	213 000	1.09

In order to understand the electrochemical dissolution mechanism of the alloys, electrolysis experiments were performed at 1.2 V and the corrosion products were characterized in solution by UV-visible spectroscopy and ESI-MS. Each electrode was immersed in 1 M HNO_3 and a constant potential (1.2 V) was applied for 2 minutes. In agreement with the linear voltammetry experiments, no gas evolution was observed and a red-brown coloration of the solution was observed.

The ESI-MS spectra of all the solutions exhibit a peak at m/z = 163 which is characteristic of TcO_4^-(m/z = 163). A representation of the ESI-MS spectrum of sample b is presented in Fig. 13

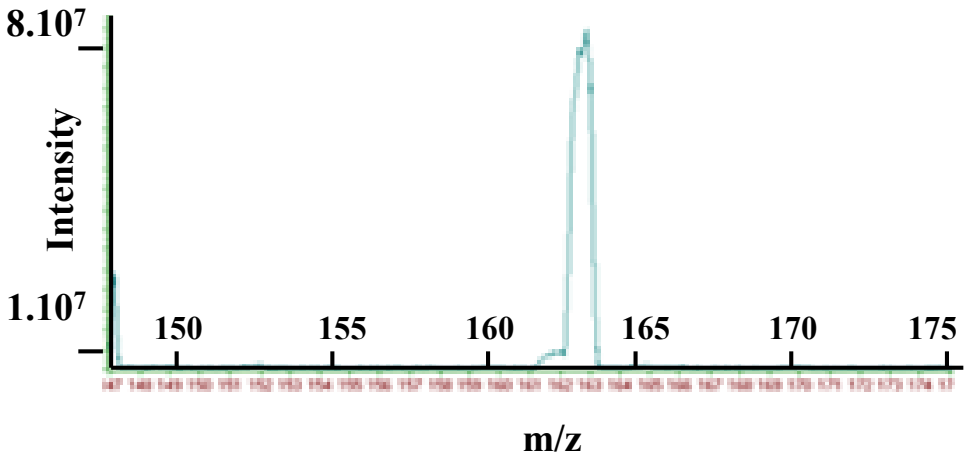

Fig. 13. ESI-MS spectra of the solutions after electrolysis of sample b at 1.2 V in 1 M HNO_3.

After electrolysis, the UV-Visible spectra of the solutions were recorded (Fig.14). The spectra exhibit a band centered at 490 nm which intensity increase with the Ru content. Ruthenium tetraoxide was not observed for Tc-Ru alloys while it was observed for Ru metal (*vide supra*). Similar phenomena has been observed during the electrochemical dissolution at 1.2 V *vs* SCE of Ru metal and Mo-Ru alloys in 1-6 M HNO_3, i.e., Ru(IV) species was observed (band at ~500 nm) for Mo-Ru alloys while RuO_4 for Ru metal.[10, 11]

Analysis of the literature indicate that red-brown Ru(IV) species can be produced from the electrochemical oxidation of $Ru(H_2O)_6^{2+}$ and its UV-visible spectra in acidic media exhibits a large band centered at 484 nm.[12, 13] X-ray absorption fine structure study in 2 M HNO_3 indicate the Ru(IV) species to be a tetramer that contains the oxo-bridged $Ru_4O_6^{4+}$ core. [13]

Further studies indicate that the dissolution of $RuO_2.xH_2O$ in 3 -10 M HNO_3 lead to a mixture tetrameric Ru(IV) /Ru(III)-nitrosyl species.[14, 15] It was mentioned that the Ru(IV) species was formed from the dissolution of $RuO_2.xH_2O$ while the Ru(III) species from the reduction of Ru(IV) with HNO_2.

In our conditions, HNO_2 is not expected which indicate that Ru(III) should not be observed and that the tetrameric Ru(IV) species should be the dominant Ru species in solution.

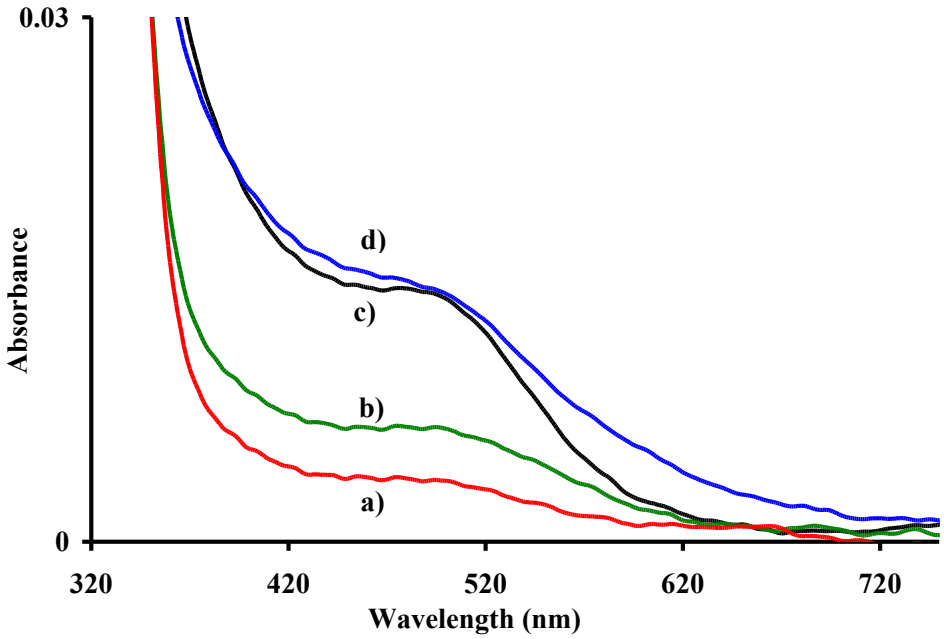

Fig. 14. UV-Visible spectra of the solution after electrolysis at 1.2 V in 1 M HNO_3 of: a) sample a in red; b) sample b in green; c) sample c in black and d) sample d in blue.

The speciation of Ru in solution during the electrochemical dissolution of Ru metal and Tc-Ru alloys can be explained considering that Ru(IV) is the primary dissolution product of Ru metal and that RuO_4 would be obtained from the oxidation of Ru(IV) by the oxygen generated from the decomposition of water. The speciation of Ru after dissolution will depend on the stability of water during the experiment, i.e., if H_2O decomposes, then RuO_4 will form from the oxidation of Ru(IV); if H_2O does not decompose, then Ru(IV) species will be present in solution. A similar mechanism has been proposed to explain the speciation of Ru after the electrochemical dissolution at 1.2 V *vs* SCE of Ru metal and Mo-Ru alloys in 1-6 M HNO_3. [11]

Because the over-potential of oxygen on Tc and Ru metal is different, it is anticipated that water will decompose at different potentials for every single alloys. It is expected that Tc-Ru alloys with low Ru content will have oxygen over-potentials comparable to the one of Tc metal (i.e., E > 1.3 V) while alloys with high Ru content will have oxygen over potentials close to the one of Ru metal (i.e., 1-1.2 V *vs* SCE). [11]

In summary, the electrochemical behavior of Tc-Ru alloys was studied for nuclear applications. Linear voltammetry experiments show that the transpassivation potentials increased significantly with the Ru content. For Ru contents below 5.2 at. %, a linear relationship between the E_{TP} and the Ru content was observed and the E_{TP} increased by ~16 mV for every at. % of Ru. For nuclear applications, a correlation between the E_{TP} and the decay time of ^{99}Tc was determined. Using the correlation, it was shown that after 1 000 and 10 000 years, the E_{TP} values would be comparable to the one of Tc metal while after one ^{99}Tc half-life the E_{TP} values would be comparable to the one of Ru metal.

3.3. Technetium-Ni alloys corrosion studies

Electrochemical measurements on Ni metal, Tc metal and Tc-Ni alloys (Tc = 1% and 10%) were performed at room temperature (20-22 °C) in 0.1 mM H_2SO_4 solutions using a computer-controlled potentiostat and frequency response analyzer. The electrochemical cell was a 100-mL flask incorporating an Ag/AgCl reference electrode and a platinized-niobium mesh counter electrode. Potentials are reported *vs*. V_{NHE}.

Open circuit potential values following 4 hours of exposure demonstrate Tc metal is approximately 150 mV greater than that of Ni metal (Fig. 15). The open circuit potentials for the 1% Tc samples appear to be statistically similar to Ni. However, the 10% Tc sample appeared to have an effect on the OCP behavior with the heat treated samples appearing to be more noble than the pure Ni sample. The addition of 10 wt% Tc to Ni appears beneficial at open circuit, but detrimental upon anodic polarization. Qualitatively, the polarizations of 10 wt% Tc alloys and composites appear like crude addition of Tc plus Ni. The 1 wt% Tc alloys behave like pure Ni, but some effect of Tc is seen upon polarization. Cathodic polarization of Tc by Ni appears feasible based on open circuit potential measurements.

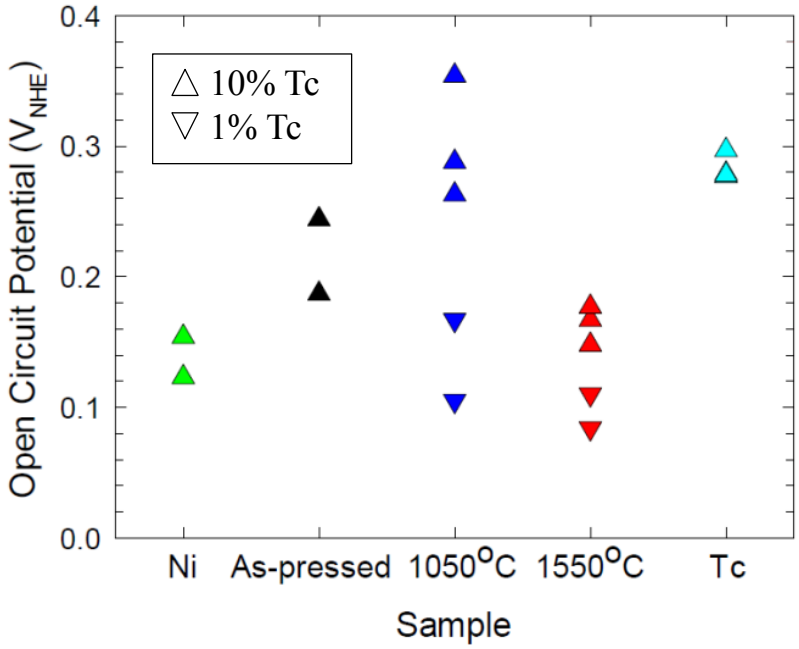

Fig. 15. Open circuit potentials for Tc-Ni samples following 4 hour exposures in 0.1 mM H_2SO_4. Color of Tc -Ni sample, Black cold pressed sample (thermally untreated). Blue: cold pressed sample and annealed at 1050 °C. Red: cold pressed sample and annealed at 1550 °C.

The similarity between the polarization resistance values of the alloys with 1 and 10 wt% Tc and the corresponding composite materials heat-treated at 1050 °C (Fig. 16) were surprising since the SEM/EDX analysis clearly showed relatively large particles of Tc metal (~10 microns) embedded in a Ni metal matrix in the composites. The polarization

resistance of the composites was expected to more closely resemble pure Ni metal with a small contribution from the relatively small exposed surface area of Tc metal. In the 1050 °C samples, it is possible that some alloying (interdiffusion) of Tc into the Ni metal occurred during heat treatment. The two samples heat-treated at 550 °C were prepared to test this possibility since any interdiffusion of the metals will be much reduced at this temperature.

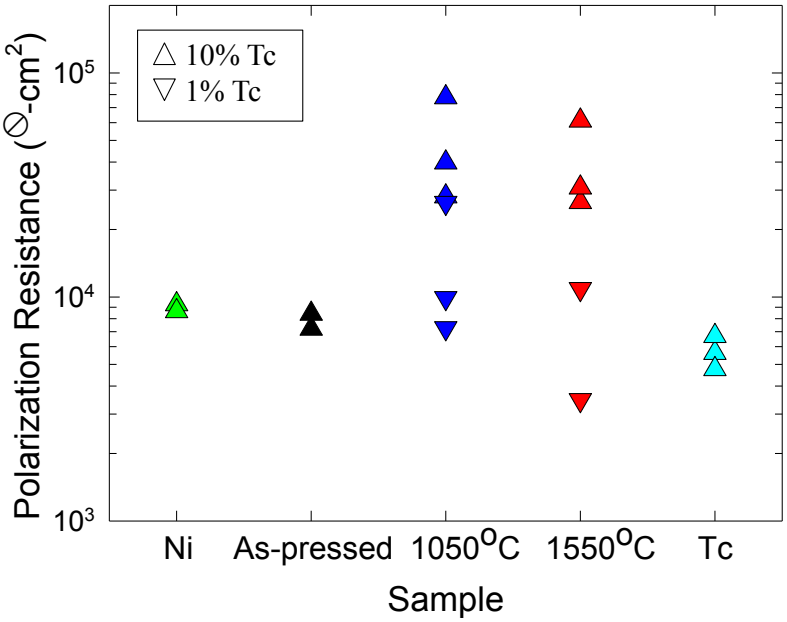

Fig. 16. Polarization resistance values Tc-Ni alloys (Tc = 1% and 10%) exposed to $3x10^{-4}$ M H_2SO_4 solution. The polarization resistance is inversely proportional to the corrosion rate.

4. Results of Task 3

4.1. Computational studies of Tc and Tc-Ru alloys.

Ab initio methods based on density functional theory have been successfully applied to investigate material properties of Tc containing systems[16, 17, 18], including Tc clusters[19], Tc and Tc-Fe surfaces[20], and bulk Tc nitrides[21].

Therefore, the same theoretical framework based on the spin-polarized density functional theory[22, 23] were used to carry out first-principles total energy calculations to investigate the materials properties of Tc and Ru metal containining materils. In thos stuides the Vienna Ab initio Simulation Package (VASP)[24] was used. The exchange–correlation energy was calculated using the generalized gradient approximation (GGA) with the parametrization of Perdew, Burke, and Ernzerhof (PBE)[25]. The Kohn-Sham (KS) equations were solved using the blocked Davidson iterative matrix diagonalization scheme followed by the residual vector minimization method. The plane-wave cutoff energy for the electronic wavefunctions was set to 300 eV. The (3x3x2) super-cell with periodic boundary conditions were used to model the bulk systems while the (2x2) slab

geometry was for the Tc(0001), RuTc (0001), and Ru(0001) surfaces. Each slab geometry consists of 5 layers for the surface calculation. The Brillouin zone was sampled using the Monkhorst-Pack scheme.[26]

The geometries of the crystal unit cells of bulk Tc, Ru, and Tc-Ru alloys were optimized at the GGA/PBE level of theory as displayed in Figure 17. For Tc, the lowest-energy structure corresponds to the HCP atomic arrangement in the space group $P6_3/mmc$, resulting in the calculated lattice parameters of a = 2.75 Å and c = 4.40 Å, that are in excellent agreement with experimental values of a = 2.743 Å and c = 4.40 Å, respectively, at ambient temperature and pressure.[27] In case of Ru, the equilibrium structure also belongs to the HCP atomic arrangement (space group $P6_3/mmc$) and its calculated lattice parameters of a = 2.72 Å and c = 4.31 Å are close to the experimental values of a = 2.75 Å and c = 4.28 Å, respectively.[28] It is also found that Tc-Ru alloys are overall random alloys and stabilized in a HCP unit cell as shown in Fig. 17. However, in case of the alloy with a Tc:Ru = 1:1, an ordered structure in the space group $P6_3/mmc$ is more stable than the case of super-lattice of two blocks of Tc and Ru superposed together, by about 0.03 eV/atom. The calculated lattice constants of the ordered Tc-Ru alloy are a = 2.74 Å and c = 4.33 Å, in excellent agreement with experimental values of a = 2.73 Å and c = 4.33 Å, respectively.[29]

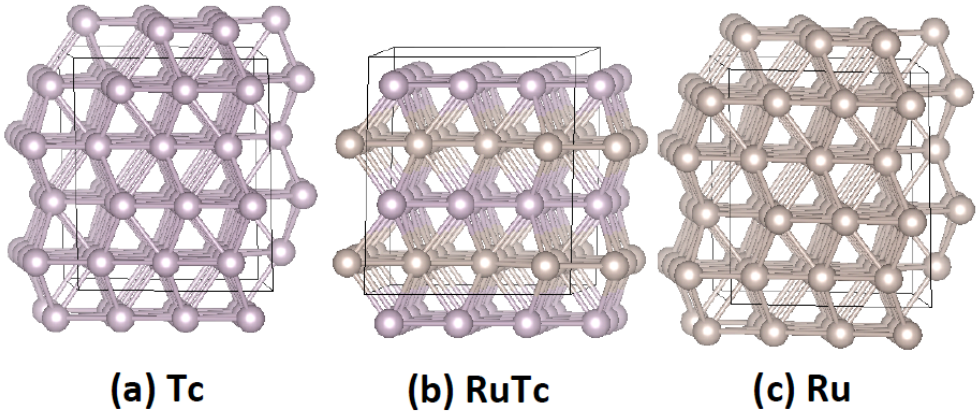

Fig. 17. Ball and stick representation of the crystal structures of : (a) Tc, (b) Ru-Tc, and (c) Ru. The Tc and Ru atoms are in silver and gold, respectively. The (3x3x2) supercells are used for bulk systems. A total of 36 atoms are included in the supercell.

The calculated lattice constants of Tc, Ru, and TcRu are shown in Table 6. Overall, the calculated values are in good agreement with the experimental values.

Other stoichiometries of Tc-Ru alloys were investigated by using the first-principles total energy method. For an alloys containing 6 at. % of Ru, (i.e., two Ru atoms in the (3x3x2) supercell), the interaction between two Ru atoms are examined by changing distance between them. It was found that those Ru atoms tend to stay away from each other in the Tc bulk system. For example, the two Ru atoms located in the third nearest neighbor distance (about 4.75 Å apart) are more stable than they are in the first nearest neighbor distance (about 2.74 Å) by 0.01 eV.

Table 6. Calculated and experimental lattice parameters of Tc and Ru metal and TcRu alloys.

	Tc		Ru		TcRu	
	DFT	Expt.	DFT	Expt.	DFT	Expt.
a (Å)	2.75	2.74	2.72	2.75	2.74	2.73
c (Å)	4.40	4.40	4.31	4.28	4.33	4.33

For Tc-Ru alloys with stoichiometry 3%Ru, 6%Ru, 25%Ru, and 50%Ru, the calculated formation energies were respectively : 6.97, 6.98, 6.99, and 7.02 eV; those results indicate a gradually increase of formation energies with the of Ru content and implies that Ru may play an important role in enhancing the bonding character in the Tc-Ru alloys.

Surface properties of Tc-Ru alloys were also investigated within the same theoretical framework as mentioned above. The (2x2) slab geometry consisting of 5 layers was used for the Tc(0001 and Ru(0001) surfaces. The effect of Ru in the Tc(0001) surface was investigated. It is found that Ru atoms tend to be located to the top most surface instead of residing in the subsurface or in the bulk. For example, a Ru atom on the top surface is energetically more favorable than on the subsurface by about 0.1 eV. When two Ru atoms are introduced in the Tc(0001) surface, the case of both Ru atoms located on the top surface is about 0.05 eV more favorable than the case of one Ru atom on the top surface and the other Ru atom on the third layer. The least favorable site for Ru atoms is on the subsurface in both cases. This is in contradiction to the case of Tc in the Ru (0001) surface. It was found that Tc atoms prefer the subsurface to the top surface or in the bulk.

In either case, results indicate that Ru atoms tend to be located on the surface, forming a protective layer on the surface of the alloys.

4.2. Computational studies of the corrosion of Tc metal

The surface chemistry of Tc metal relative to hydrogen, oxygen and water molecule adsorption was studied by DFT. For Tc metal, four different atomic adsorption sites are possible on Tc (0001) : (i) on-top site, (ii) a bridge site between two surface Tc atoms, (iii) a hexagonal-close-packed (HCP) hollow site when there is a Tc atom in the layer directly beneath the surface layer, and (iv) a face-centered-cubic (FCC) hollow site when there is a hole in the layer directly beneath the surface layer (Fig. 18). Hydrogen, oxygen, and water sorption was evaluated.

The findings indicate that the preferable adsorption sites strongly depend on the adsorbates. No physisorption sites for hydrogen and oxygen molecules are identified on the Tc (0001) surface. The calculated oxygen adsorption energy on Tc(0001) is in excellent agreement with 3.67 eV/atom from the previous studies. Water adsorption on the Tc(0001) surface is also elucidated, revealing its dissociation products (H^+ and OH^-). The Eh-pH diagram of the system Tc-O-H was constructed by solving the Nernst equations for possible reactions between Tc and its oxidizing products. The available

experimental data taken for Tc, TcO_2 and TcO_4^- fall nicely into the estimated stability region at pH = 4.

The hydrogen adsorption energies are calculated at the several possible adsorption sites (on the Tc(0001) surface. Both atop and bridge sites are less energetically stable. In order to calculate hydrogen adsorption energies the total energy of the system consisting of an isolated hydrogen molecule above the Tc (0001) surface is taken as a reference (Fig. 26). A hydrogen molecule splits into two hydrogen atoms on the Tc(0001) surface. Adsorption energies are within the range of 0.56 to 0.71 eV per hydrogen atom, depending on the adsorption sites. The most energetically favorable site for hydrogen atoms is the FCC hollow site (0.71 eV/H), followed by the HCP hollow site (0.68 eV/H), as depicted in the Fig. 26. The least favorable case corresponds to one hydrogen atom sitting on a HCP hollow site while the other occupies a FCC hollow site, as depicted in Fig. 18 (c). The calculated bond lengths of Tc-H are in the range 1.90 -1.95 Å when hydrogen sits on the FCC hollow site. No physisorption sites are identified in this study, implying that the Tc(0001) surface serves as a strong catalyst for hydrogen. The calculated bond energy of a hydrogen molecule is 4.44 eV, in good agreement with the experimental value of 4.52 eV [30] and a previously reported theoretical value of 4.57 eV [31].

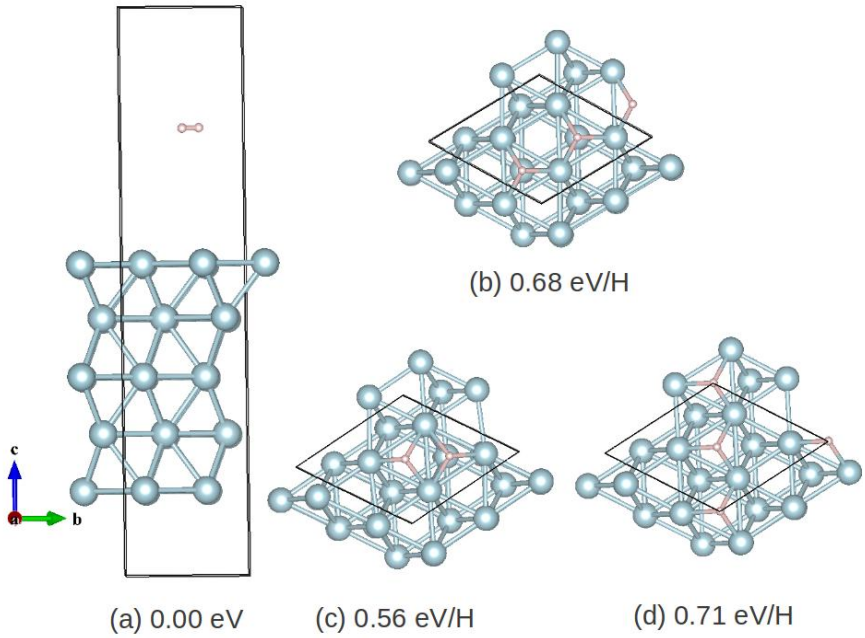

Fig. 18. Hydrogen on Tc(0001): a. H_2 above Tc(0001), b. two H atoms on HCP hollow sites, c. one H atom on HCP hollow site and one H atom on FCC hollow site, and d. two H atoms on FCC hollow site.

The adsorption energies of oxygen on the Tc(0001) surface are also calculated for several possible adsorption sites (Fig. 19). The total energy of an isolated oxygen molecule on the Tc(0001) surface is taken as a reference. An oxygen molecule splits into two oxygen atoms on the Tc (0001) surface, gaining energy of 2.09 to 3.61 eV per oxygen. The most energetically favorable case corresponds to both oxygen atoms on HCP hollow sites (3.61 eV/O) followed by the case with one oxygen sitting on a HCP

hollow site while the other occupies a FCC hollow site (3.01 eV/O). The least favorable case is for both oxygen atoms located atop (2.09 eV/O). Both hydrogen and oxygen are less favorable to occupy atop and bridge sites. However, unlike the hydrogen adsorption, in which hydrogen prefers the FCC hollow site (0.71 eV/H), oxygen prefers the HCP hollow site (3.61 eV/O) on the Tc(0001) surface. No physisorption is identified for oxygen on the Tc(0001) surface.

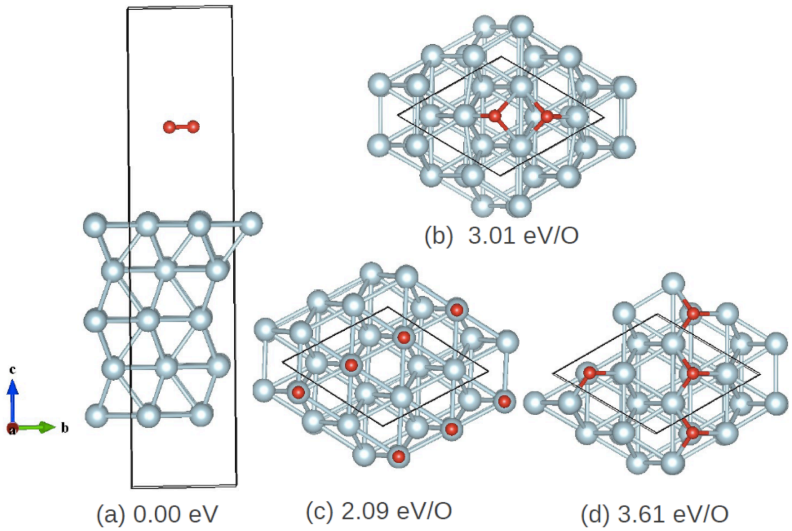

Fig. 19. Oxygen on Tc(0001): a. O_2 above Tc(0001), b. O atoms on HCP hollow sites and FCC hollow site, c. two O atoms atop and d. two O atoms on HCP hollow site

The findings indicate that, unlike in the case of hydrogen and oxygen molecules, physisorption of water is possible on the Tc(0001) surface (Fig. 19) leading to a gain of 0.40 eV/H_2O compared to the total energy of an isolated water molecule above the Tc (0001) surface. However, the molecule can eventually split into OH and H. Physisorptions of oxygen and hydrogen molecules on the Tc(0001) surface were not observed in this study. The estimated chemisorption energies are in the range 0.61-1.34 eV/H_2O, depending on the adsorption sites. Overall OH tends to be located on the HCP hollow site, while H prefers the FCC hollow site.

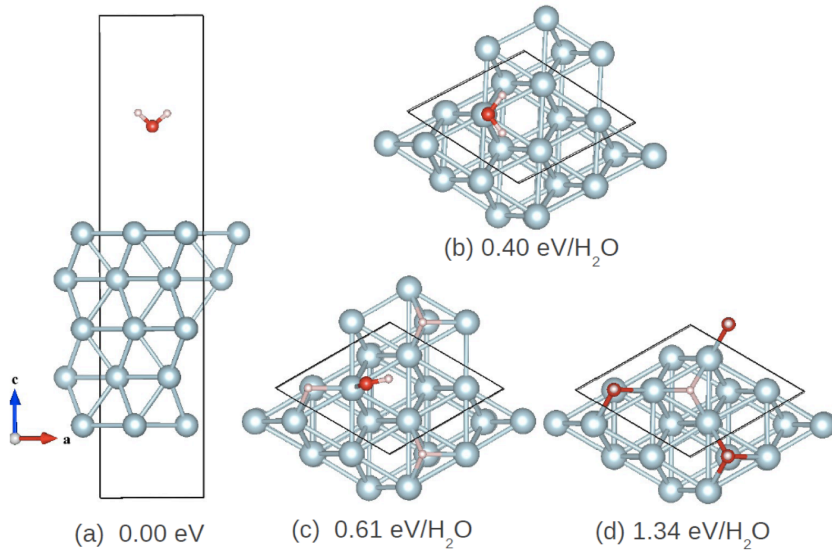

Fig. 20. Water on Tc(0001): a. water molecule on Tc(0001) surface, b. atop, c. OH atop and H at the HCP hollow site and d. OH at HCP hollow site and H at the FCC hollow site.

Corrosion is a natural process that degrades materials properties, facilitated by electrochemical processes occurring in aqueous conditions due to the interaction between the metal and the moisture. On the basis of the DFT studies, hydrogen and hydroxide are the most probable dissociation products from water on Tc(0001) surface as discussed above. Stability of water and its dissociation products (H and OH) when in contact with Tc(0001) can be estimated from the equilibrium potentials by solving the Nernst equations[32, 33] as a function of acidity. The results can also be compared to the available experimental data. The adsorption geometries of water and its dissociation products are determined at 0 V from DFT.

The DFT calculations indicate that water splitting cathodic reaction ($2H_2O_{(l)} + 2e^- \rightarrow H_2 + 2OH^-$) can occur directly on Tc (0001), in neutral waters. One common cathodic reaction encountered during the corrosion of metals is the oxygen reduction : $O_2 + 4H^+ + 4e^- \rightarrow 2H_2O$. The equilibrium potential (E^0) between Tc and its various oxidized species as a function of pH can be used to map out the lines of equilibrium between different reactions as potential and acidity are varied (Fig. 21). In the Tc-O-H system, only the two possible reactions, in equilibrium with solid Tc, are considered in this case ($TcO_2 + 4H^+ + 4e^- \rightarrow Tc + 2H_2O$ and $TcO_4^- + 8H^+ + 7e^- \rightarrow Tc + 4H_2O$). The experimental data collected for Tc (solid circle), TcO_2 (solid square), and TcO_4^-(solid diamond) at pH = 4 are in the region of the calculated stability for each species. [34] The equilibrium between TcO_2 and TcO_4^-would make the slope of the line steeper than in the case between TcO_2 and Tc (red). The equilibrium potentials are 0.747 V (the former) and 0.472 V (the later), respectively, at pH = 0.

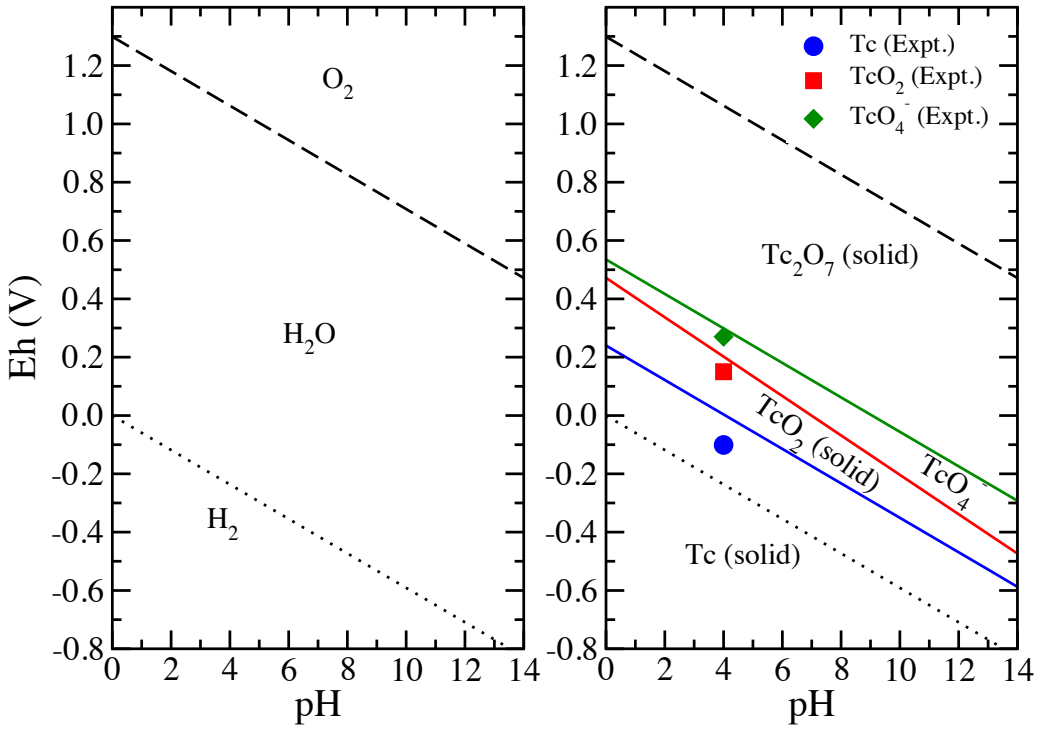

Fig. 21. Eh-pH diagram for pure water (left) and the Tc-O-H system (right) at 1.0 M, 298.15 K and 1 atmosphere. For the Tc system products include TcO_2 and TcO_4^-.

4.3. Computational studies of Tc-oxides

Because Tc-Fe -oxide could form on the surface of alloys containing Fe (i.e., Inconel) a systematic study on the structures and properties of three Tc-Fe oxide systems, in cubic, othorhombic, and rhombohedral lattices, was performed. The standard spin-polarized density functional theory was employed to calculate the total energies and lattice constants. The findings indicate that magnetite can host Tc atoms up to about 33%, forming a $TcFe_2O_4$ spinel. The calculated inclusion energies are -0.76 eV/Tc for one $FeFe_2O_4$ molecule and -0.97 eV/Tc for eight $FeFe_2O_4$ molecules converting into $TcFe_2O_4$, respectively. Above 33% of Tc inclusion, a $TcFe_2O_4$ spinel becomes energetically even less stable than the ones in $CaFe_2O_4$ and YFe_2O_4 lattices. Atomistic investigations carried out for binary Tc oxides including TcO, TcO_2, TcO_3, and Tc_2O_7 indicate that TcO_2 is the most energetically favorable form of Tc oxides, followed by Tc_2O_7. A systematic study carried out for three iron oxides, when Tc inclusion occurs, using the standard spin-polarized density functional theory, predicts that magnetite can host Tc atoms up to about 33%, forming a $TcFe_2O_4$ spinel. The Tc inclusion energies in the bulk iron and magnetite were calculated.

The benchmark calculation was carried out for magnetite (Fe_3O_4) by varying the effective strong-electron correction parameter, U_{eff}, to correct for the lack of electron localization within the framework of standard DFT. The results are compared to experimental data, as summarized in Table 7. The estimated lattice constant is

underestimated when U_{eff} = 0 eV while it is slightly overestimated when U_{eff} = 2 and 4 eV, compared to the experimental value of 8.39 Å. The volume compression data also show that the calculated volume is consistently overestimated when the U_{eff} value is greater than or equal to 1, as shown in Fig. 22. This finding indicates that the LDA+U correction may be necessary to predict the structural properties of Tc incorporated iron oxides accurately. The calculated total energy of magnetite implies that Tc may be incorporated in magnetite up to about 33%, forming a $TcFe_2O_4$ spinel; however, the spinel structure becomes very unstable upon additional Tc incorporation due to the appearance of $TcTc_2O_4$.

Table 7. Lattice constant and bulk modulus of magnetite. Units are in Å and GPa for the lattice constant and bulk modulus, respectively.

U_{eff} (eV)	0	2	4	Expt.
Lattice constant (Å)	8.37	8.43	8.45	8.39
Bulk modulus (GPa)	173	176	178	180

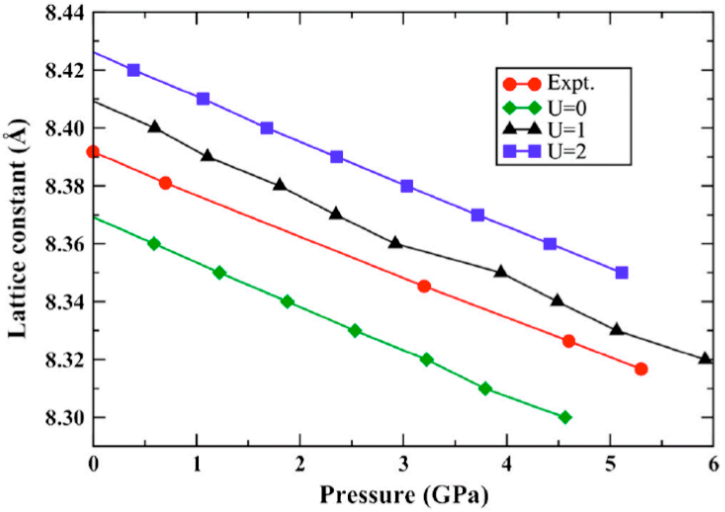

Fig. 22. Compressibility of magnetite from published data.

The Tc incorporation energy in magnetite was calculated as follows:

$$E_{Tc}^{i}\,(\text{Magnetite}) = [E^{tot}\,(FeFe_2O_4) + n\,E^{tot}\,(Tc1)] - [E^{tot}\,(TcFe_2O_4) + n\,E^{tot}\,(Fe1)]$$

$$E_{Tc}^{i}\,(Fe) = [E^{tot}\,(Fe16) + n\,E^{tot}\,(Tc1)] - [E^{tot}\,(Tc_nFe_m) + n\,E^{tot}\,(Fe1)]$$

where $E^{tot}(FeFe_2O_4)$ and $E^{tot}(TcFe_2O_4)$ represent the total energies of magnetite and $TcFe_2O_4$, respectively. Each has eight formula units (f. u.) in the unit cell. E^{tot} *(Tc1)* and E^{tot}*(Fe1)* are total energies of a single atom of Tc and Fe, respectively. E^{tot} *(Fe16)* corresponds to the total energy of bulk iron in a (2x2x2) unit cell including 16 atoms. Here, n and m are the numbers of Tc and Fe atoms in the alloys, resulting in $n+m$ = 16. The calculated Tc inclusion energy in bulk iron is -0.17 eV per Tc atom when a Tc atom replaces a Fe atom in the (2x2x2) unit cell consisting of 16 Fe atoms. This indicates that

the reaction is endothermic. There are eight molecules of $FeFe_2O_4$ in magnetite. Similarly, converting one $FeFe_2O_4$ molecule to one $TcFe_2O_4$ molecule requires -0.76 eV per Tc, which gradually increases to -0.97 eV per Tc until all of the $FeFe_2O_4$ are converted into $TcFe_2O_4$. Iron oxides are known to be strongly correlated systems, thus DFT+U is crucial to accurately predict structural, as shown in Table 7. Therefore, further investigation to assess the strong electron corrections in iron oxides under consideration is necessary to validate our findings qualitatively and quantitatively. It is found that using the value, U = 2, the estimated lattice constant and bulk modulus of magnetite can be improved significantly.

5. Publications and presentations

1. *Electrochemical studies of technetium-ruthenium and rhenium-ruthenium alloys in nitric acid: Implications for the long term behavior of metallic technetium waste forms.* Farmand. R.; Poineau. F.; Jarvinen. G.; Kolman. D.G.; Koury. D.J.; Czerwinski. K. R. 248th ACS National Meeting & Exposition, San Francisco, CA, United States, August 10-14, 2014 (2014), NUCL-90.

2. *Electrochemical studies of technetium-ruthenium and rhenium-ruthenium alloys in nitric acid: implications for the long-term behavior of metallic technetium waste forms.* Farmand. R.; Poineau. F.; Koury. D.J.; Kolman. D.G.; Jarvinen. G; Czerwinski. K. R. 8th International Symposium on Technetium and Rhenium: Science and Utilization. La Baule -Pornichet, France 29th sept. -3rd oct (2014).

3. *The aqueous corrosion behavior of technetium -alloy and composite materials.* Jarvinen, G.; Kolman, D.; Taylor, C.; Goff, G.; Cisneros, M.; Mausolf, E.; Poineau, F.; Koury, D.; Czerwinski, K. International Nuclear Fuel Cycle Conference, Salt Lake City, UT, United States, Sept. 29-Oct. 3, 2013 (2013), 2, 1138-1144.

4. *First-principles and kinetic Monte Carlo simulation studies of the reactivity of Tc(0001), MoTc(111) and MoTc(110) surfaces*. Kim. E.; Weck. P. F.; Taylor. C.D.; Olatunji-Ojo. O.; Liu. X. Y; Mausolf. E.; Jarvinen. G. D.; Czerwinski, K.R. J. Electrochem. Soc. (2014), 161(3), C83-C88.

5. *Thermodynamics of technetium: reconciling theory and experiment using density functional perturbation analysis*. Weck. P. F.; Kim. E. Dalton Trans. (2015), 44(28), 12735-12742.

6. *Electrochemical studies of technetium-ruthenium alloys in HNO_3: Implications for the behavior of technetium waste forms.* F. Poineau, D. Koury, J. Bertoia, D.G. Kolman, G.S. Goff, E. Kim, G. Jarvinen, K.R. Czerwinski. 2016, Submitted, Radiochemistry.

6. Financial

FY	*FY13*	*FY14*	*FY15*	*FY16*
total	*$247,333*	$294,329	*$236,476*	*$11,344*
cumulative	*$247,333*	$541,662	*$778,138*	*$789,482*

7. References

[1] F. Poineau, E. Mausolf, G. D. Jarvinen, A. P. Sattelberger, and K. R. Czerwinski, *Inorg. Chem*., **52**, 3573 (2012).

[2] E. C. Buck, E. J. Mausolf, B. K, McNamara, C. Z. Soderquist, and J. M Schwantes, *J. Nucl. Mater*., **461,** 236 (2015).

[3] G. D. Jarvinen, K. M. Long, G. S. Goff, W. H. Runde, E. J. Mausolf, K. R. Czerwinski, F. Poineau, E. P. McAlister, and P. Horwitz, *Solv. Extr. Ion. Exch*., **31**, 416 (2013).

[4] S. A. Luksic, B. J. Riley, M. Schweiger, and P. Hrma, *J. Nucl. Mater*., **66**, 526 (2015).

[5] F. Poineau, T. Hartmann, P. F. Weck, E. Kim, G. W. C. Silva, G. D. Jarvinen, and K. R. Czerwinski, *Inorg. Chem*., **49**, 1433 (2010).

[6] W. L. Eber, J. C. Cunnane, S. M. Frank, and M. J. Williamson. Immobilization of Tc in a metallic waste form, in Materials Challenges in Alternative and Renewable Energy. G. Wicks, J. Simon, R. Zidan, E. Lara-Curzio, T. Adams, J. Zayas, A. Karkamkar, R. Sindelar and B. Garcia-Diaz, Editors. American Ceramic Society, 2011, 291-304.

[7] C. D. Taylor and X. Y. Liu, *J. Nucl. Mater*., **434**, 382 (2013).

[8] J. B. Darby, A. F. Berndt, and J. W. Downey. *J. Less-Common Metals*. **9**, 466 (1965).

[9] K. V. Rotmanov, A. G. Maslennikov, E. M. Pichuzhkina, and V.F. Peretrukhin, *Radiochemistry*, **57**, 131 (2015).

[10] A. Maslennikov, B. Fourest, F. David, and M. Masson, *Radiochim. Acta*, **91**, 419 (2003).

[11] A. Maslennikov, B. Fourest, F. David, and M. Masson, *Radiochim. Acta*, **91**, 761 (2003).

[12] A. Patel and D. T. Richens, *Inorg. Chem*., **30**, 3789 (1991).

[13] J. R. Osman, J. A. Crayston, and D. T. Richens, *Inorg. Chem*., **37**, 1665 (1998).

[14] F. Mousset, C. Eysseric, and F. Bedioui, Studies of dissolution solutions of ruthenium metal, oxide and mixed compounds in nitric acid. ATALANTE 2004, Nîmes (France), June 21-25, 2004.

[15] F. Mousset, F. Bedioui, and C. Eysseric, *Electrochem. Commun.*, **6**, 351 (2004).

[16] P. F. Weck, E. Kim, F. Poineau, E. E. Rodriguez, A. P. Sattelberger, and K. R. Czerwinski, *Dalton Trans*. 39, 7207 (2010).
[17] P. F. Weck, E. Kim, F. Poineau, and K. R. Czerwinski, *Phys. Chem. Chem. Phys*.**11**, 10003, (2009).
[18] P. F. Weck, E. Kim, F. Poineau, E. Rodriguez, A. Sattelberger, and K. R. Czerwinski, *Inorg. Chem*. **48**, 6555 (2009).
[19] P. F. Weck, E. Kim, K. R. Czerwinski, *Chem. Phys. Lett*. **487**, 190 (2010).
[20] C. D. Taylor, *J. Nuclear. Mater*. **408**, 183 (2011).
[21] P. F. Weck, E. Kim, and K. R. Czerwinski, *Dalton Trans*. 40, 6738 (2011).
[22] P. Hohenberg and W. Kohn, *Phys. Rev*. **136**, B864 (1964).
[23] W. Kohn and L. J. Sham, *Phys. Rev*. **140**, A1133 (1965).
[24] G. Kresse and J. Furthmuller, *Phys. Rev. B: Condens. Matter*, 1996, 54, 11169.
[25] P. Perdew, K. Burke, and M. Ernzerhof, *Phys. Rev. Lett*. **77**, 3865 (1996).
[26] H. J. Monkhorst and J. D. Pack, *Phys. Rev. B* 13, 5188 (1976).
[27] D. J. Lam et al., *Nature*, 192, **744** (1961).
[28] Y. Urashima et al., *Mineralogical Journal*, **7**, 438 (1974).
[29] J. B. Darby et al., *J. Less-Common Metals* 5, 397 (1963).
[30] D. R. Lide, CRC Handbook of Chemistry and Physics, 76th ed. CRC Press, New York, 1996.
[31] P. Ferrin, S. Kandoi, A. U. Nilekar, and M. Mavrikakis, Surf. Sci. 606, 679 (2012).
[32] M. V. Orna and J. Stock, John (1989). *Electrochemistry, past and present*. Columbus, OH: American Chemical Society.
[33] D. Wahl, *Galvanotechtnik* **96** (8): 1820–1828 (2005).
[34] E. Mausolf, "Separation of Tc from U and Development of Metallic Tc Waste Forms" (2013). UNLV Thesis/Dissertations/Professional Papers/Capstones. Paper 1860. (http://digitalscholarship.unlv.edu/thesesdissertations/1860)